

The use of the autoencoder to improve images in ultrasound tomography

Abstract. The article presents the idea of a system enabling effective control of industrial processes. The high level of automation and processes monitoring plays a key role in maintaining the competitiveness of each enterprise. The paper presents an innovative approach to industrial ultrasound tomography. A shallow neural network enriched with an autoencoder was used to visualize the 2D cross-section of the tank (reactor) filled with tap water. The novelty is the use of an autoencoder to improve the quality of the measurement vector

Streszczenie. W artykule przedstawiono ideę systemu umożliwiającego efektywną kontrolę procesów produkcyjnych. Wysoki poziom automatyzacji i monitorowania procesów produkcyjnych odgrywa kluczową rolę w utrzymaniu konkurencyjności każdego przedsiębiorstwa. W artykule przedstawiono nowatorskie podejście do przemysłowej tomografii ultradźwiękowej. W celu zobrazowania dwuwymiarowego przekroju zbiornika (reaktora) wypełnionego wodą z kranu wykorzystano płytką sieć neuronową wzbogaconą o autoenkoder. Nowością jest zastosowanie autoenkodera do poprawy jakości wektora pomiarowego. (Zastosowanie autoenkodera do poprawy jakości obrazów w tomografii ultradźwiękowej).

Keywords: electrical impedance tomography, elastic net, inverse problem.

Słowa kluczowe: elektryczna tomografia impedancyjna, elastic net, problem odwrotny.

Introduction

Ultrasound tomography (UST) is a relatively uncommon imaging technique that can be used to diagnose industrial processes, including reactors and tanks. The advantages of this method include security for staff and processes, non-invasiveness, speed of operation and low costs of using UST technology. Due to the non-invasive nature of UST, this method has great potential for use in various areas of the economy. In particular, these are the following fields of application: food and chemical industry, production of detergents, paints and cosmetics, pharmaceutical industry etc. Industrial processes are usually characterized by high variability (dynamics), which is why imaging speed is an important factor in monitoring systems. The most popular techniques used in industrial tomography include: electrical tomography, computed tomography (CT) [1] and radio tomography (RT) [2]. Electrical tomography can be divided into electrical impedance tomography (EIT) [3,4], electrical resistivity tomography (ERT) and electrical capacitance tomography (ECT) [5–10].

Ultrasound/ultrasonic tomography (UST) is one of the less common methods in industrial applications, but it is very popular in medical imaging [11]. This fact indicates the existence of available potential of UST in industry. To meet expectations in the field of imaging speed, while maintaining high quality tomographic images, the described research uses the shallow feedforward neural network.

There are many methods for solving optimization problems [12–19]. The novelty of the presented approach is the use of an autoencoder to reduce the noise of the measurement vector [20]. In the described case, the input vector contained 496 measurements. The output image was displayed on a monochrome monitor with a resolution of 32×32 (1024 pixels). The basic reconstruction algorithm operates based on a neural network with the following structure: 496 (inputs) - 1024 (hidden neurons) - 1024 (output neurons) - 1024 (real output values).

Materials and methods

As it was previously mentioned the research described in this article use a method based on artificial neural network (ANN) preceded by an autoencoder. The measurement vector constituting the ANN input consists of 496 measurements. Each of the measurements reflects the

time in which the sound wave travels the distance between individual transducers. Each of the 32 transducers located around the walls of the container can both emit and receive ultrasound signals. If there are no inclusions in the sound wave path, the time is the shortest. Before starting the measurements, the system performs the reference measurement in an inclusion-free environment. In this way, the appearance of inclusions interferes with (decreases) the speed of sound, thus increasing the time recorded between the individual transducers. This allows you to determine the location and size of the inclusions.

The test object is a physical model of an industrial container. During the research, the container filled with tap water was used. Different inclusions were hidden in the water and ultrasound measurements were performed. Knowledge of location and dimensions, as well as the number of all inclusions corresponding to each measurement, enabled the development of a simulation algorithm that generated 20,000 simulation cases (measurements and pattern images).

Fig. 1 presents the test stand that was used for validation of the simulation algorithm. The stand consists of a tank filled with tap water. 32 transducers which can generate ultrasound waves and receive them were placed around the tank. Plastic tubes of various diameters, in various quantities and in different positions relative to each other were immersed in water. At the bottom of the tank you can see numbered markings enabling the location of individual inclusions.



Fig. 1 The test stand with 32 transducers arranged around the bucket

Fig. 2 visualizes an example of a simulation of generating one of 20,000 measurement cases. The figure shows an example of a cross-section of a container with visible inclusions. Each separate case taking into account a specific distribution of inclusions has a different distribution of measurement values. Because of this, ANN and autoencoder can capture the relationship between the values of individual elements of the measurement vector (inputs) and the values of the pixels of the output image.

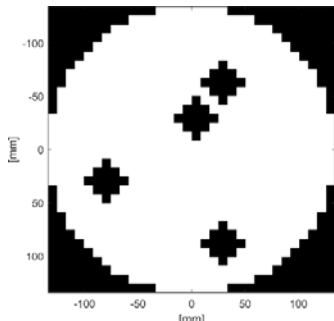


Fig. 2 example of a cross-section of a container with visible inclusions

Designing autoencoder architecture

Autoencoder is a special kind of neural network that is trained in input replication at the output. Autoencoders can be used as data denoise tools as well as for training neural networks. Autoencoder training is done without supervision in the sense that one set of data is used, without using any reference data (patterns) [21]. The training process is still based on the optimization of penalties (cost values). The penalty function measures the error between input x and its reconstruction at the output \hat{x} . The autoencoder consists of an encoder and a decoder. The encoder and decoder can have many layers, but in presented research it was assumed that each of them has only one layer. If the input layer is a vector $x \in \mathbb{R}^{D_x}$ then the encoder converts the vector x to another vector $z \in \mathbb{R}^{D^{(1)}}$ as follows (1):

$$z = h^{(1)}(W^{(1)}x + b^{(1)}) \quad (1)$$

where $h^{(1)}: \mathbb{R}^{D^{(1)}} \rightarrow \mathbb{R}^{D^{(1)}}$ is the encoder transfer function; $W^{(1)}: \mathbb{R}^{D^{(1)} \times D_x} \rightarrow \mathbb{R}^{D^{(1)}}$ is the weight matrix; $b^{(1)} \in \mathbb{R}^{D^{(1)}}$ is a bias vector; the superscript (1) means the first layer of autoencoder.

Strengthening the sparsity autoencoder is achieved by adding a stabilizer to the cost function. The regulatory element is a function of the mean baseline value of neuron activation. The average value of the neural output activation i is defined as (2):

$$\hat{\rho}_i = \frac{1}{n} \sum_{j=1}^n z_i^{(1)}(x_j) = \frac{1}{n} \sum_{j=1}^n h(w_i^{(1)T} x_j + b_i^{(1)}) \quad (2)$$

where x_j is the j^{th} training example; n is the overall number of training examples; $w_i^{(1)T}$ is the i^{th} row of the weight matrix $W^{(1)}$; $b_i^{(1)}$ is the i^{th} entry of the bias vector, $b^{(1)}$.

A neuron is considered 'fired' if its output power activation value is high. A low output activation value means that the neuron in the hidden layer 'fires' in response to a small number of training examples. Adding this term to the cost function, which limits $\hat{\rho}_i$ to a low level, encourages the auto encoder to learn representation, where each neuron in the hidden layer launches a small amount of training cases.

This means that each neuron specializes in a function that is only present in a small subset of training examples.

The sparsity regulator attempts to force the sparsity limit to exit from the hidden layer. Parameterization can be supported by adding a regularization term, which takes a high value when the average value $\hat{\rho}_i$ of neuron activation i and its desired value ρ is not close to the value (cost function) [22]. One such term for sparse regularization Ω_s may be the Kullback-Leibler divergence which can be transformed into the form (3).

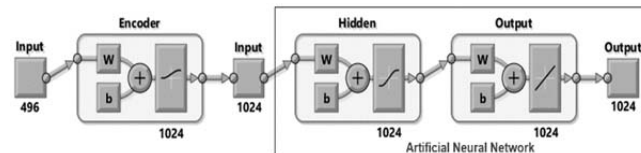


Fig. 3 ANN preceded by an encoder.

$$\Omega_s = \sum_{i=1}^{D^{(1)}} \rho \log\left(\frac{\rho}{\hat{\rho}_i}\right) + (1-\rho) \log\left(\frac{1-\rho}{1-\hat{\rho}_i}\right) \quad (3)$$

where: $D^{(1)}$ is the number of neurons in the encoder output; $\hat{\rho}_i$ is the mean activation value of neuron i ; ρ is desired value.

The Kullback-Leibler divergence is a function for measuring the difference between two distributions. In the presented case it takes the value zero, when ρ and $\hat{\rho}_i$ are equal. If they differ, they become larger. Minimizing the criminal function forces the term to be small. Therefore, the values of ρ and $\hat{\rho}_i$ are close to each other. An average activation value of 0.05 was used during autoencoder training. The penalty (cost function) used to train a sparse autoencoder is an adjustable function of the mean square error, which can be represented in the following form (4):

$$E = \underbrace{\frac{1}{N} \sum_{n=1}^N \sum_{k=1}^K (x_{kn} - \hat{x}_{kn})^2}_{\text{mean squared error}} + \underbrace{\lambda \cdot \Omega_w}_{L_2 \text{ weights regularization}} + \underbrace{\beta \cdot \Omega_s}_{\text{sparsity regularization}} \quad (4)$$

where β is the coefficient for the scarcity settlement period and λ is the coefficient for the L_2 settlement period. During autoencoder training, the values of these coefficients were as follows: $\lambda = 0.005$ and $\beta = 1.2$. In formula (4) the expression $\lambda \cdot \Omega_w$ is the L_2 norm for weight regulation, and $\beta \cdot \Omega_s$ is the sparsity factor for regularization.

During the sparse autoencoder training process, the size of the sparse regulator can be reduced. This is done by simultaneously increasing the weight $w^{(1)}$ values and reducing the values of $z^{(1)}$. To prevent this, add the term "weight adjustment" to the cost function. This term is called the L_2 regularization term Ω_w and is defined by (5):

$$\Omega_w = \frac{1}{2} \sum_l^L \sum_j^n \sum_i^k (w_{ij}^{(l)})^2 \quad (5)$$

where L is the number of hidden layers; n is the number of observations (cases); k is the number of variables in the data set.

In addition to the autoencoder, UST images were reconstructed using a classic artificial neural network (ANN) with a multilayer perceptron structure with only one hidden layer. The neural network contained 469 inputs, one hidden layer with 1024 neurons, 1024 neurons in the output layer and 1024 outputs in real numbers. 1024 output values are converted to a 32×32 pixel image. 496 measurements must be enough to reproduce 1024 pixels, which means that we are dealing with a vague problem. The entire data set consisted of 20,000 cases generated by a simulation

algorithm. These were measurements of the propagation time of sound waves in the tested tank expressed in $[\mu\text{s}]$. The data set has been divided into 3 subsets: training set, validation set and testing set in the proportions 70:15:15.

Fig. 3 shows the structure of a hybrid network consisting of an encoder and an ANN. The encoder input contains a vector of 496 measurements. It is encoded on 1024 outputs, which constitute the input to the ANN. ANN is a multilayer perceptron with 1024 neurons in the hidden layer, 1024 neurons in the output layer and 1024 output values. By encoding 496 measurements to more features, the incompleteness problem has been solved.

Results

Figures 4-6 show a comparison of image reconstruction obtained using ANN only, and ANN enhanced with an encoder. Five selected reconstructions were compared, differing in the number of inclusions, size and location in relation to the walls of the tested tank. Column (2) contains pattern images. Column (3) shows the reconstruction results generated by pure ANN (without encoder). It can be seen that all the images in the column (3) are very noisy, although they contain outlines of inclusions. Column (4) presents the results of reconstructions obtained using ANN enhanced by encoder. Most of the noise has been removed this way.

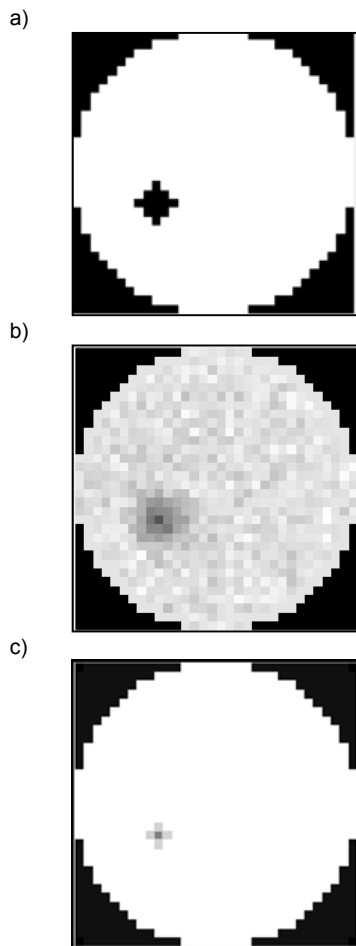


Fig.4. Image reconstructions – model I: a) pattern, b) direct ANN reconstruction, c) ANN reconstruction enhanced by encoder

Thanks to the use of encoder prior ANN, the inclusions are clearly visible and precisely mapped. In the case where the inclusion is small, the algorithm mapped it slightly less in contrast than in the reference image. However, it is still visible.

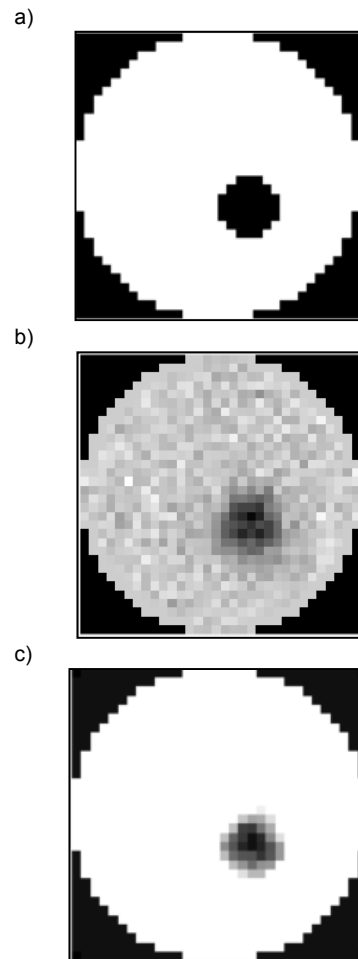
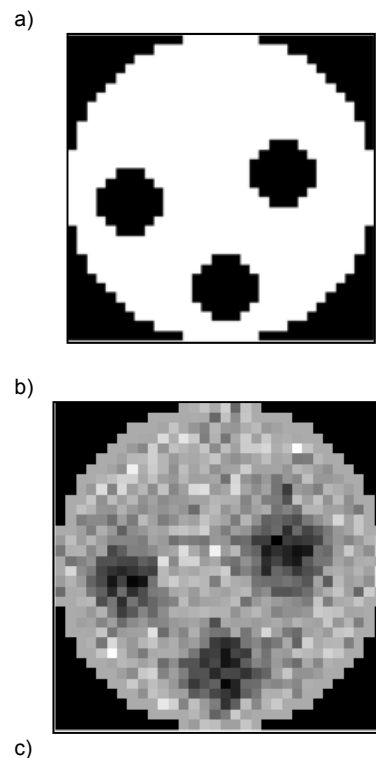


Fig.5. Image reconstructions – model II: a) pattern, b) direct ANN reconstruction, c) ANN reconstruction enhanced by encoder



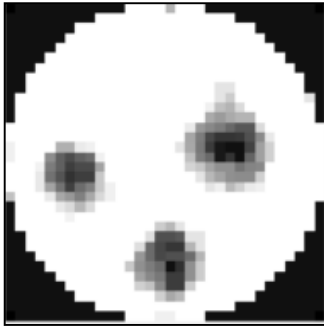


Fig.6. Image reconstructions – model III: a) pattern, b) direct ANN reconstruction, c) ANN reconstruction enhanced by encoder

Conclusions

The article presents an original concept of using a neural network enhanced with an autoencoder to denoise input data. The presented research used ultrasound tomography to identify hidden inclusions in a water-filled tank. The input vector contained 496 measurements that were characterized by high level of noise. The source of noise were errors and inaccuracies in measuring devices, as well as interference in the way of data transfer between particular elements of the measuring system. Studies have shown that using conventional ANN, the resulting reconstruction images are blurred and out of focus. The sparse encoder located in front of the ANN inputs, significantly improves the quality of the measurement data. In addition, the use of an encoder in a sufficiently large number of neurons allows the conversion of an undercomplete problem to overcomplete, which expressively improves reconstruction results. Our research confirmed that the use of sparse autoencoders can significantly improve tomographic imaging results. Thanks to this, the UST method, which is not widely used, can be successfully used in industry.

Authors: Tomasz Rymarczyk, Ph.D. Eng., University of Economics and Innovation, Projektowa 4, Lublin, Poland, E-mail: tomasz@rymarczyk.com, Grzegorz Kłosowski, Ph.D. Eng., Lublin University of Technology, Nadbystrzycka 38A, Lublin, Poland, E-mail: g.klosowski@pollub.pl; Tomasz Cieplak, Ph.D., Lublin University of Technology, Nadbystrzycka 38A, Lublin, Poland, E-mail: t.cieplak@pollub.pl; Edward Kozłowski, Ph.D., Lublin University of Technology, Nadbystrzycka 38A, Lublin, Poland, E-mail: e.kozlowski@pollub.pl; Konrad Kania, WSEI/Netrix S.A., E-mail: konrad.kania@netrix.com.pl.

REFERENCES

- [1]. About L., Grudzień K., Wiącek J., Niedostatkiwicz M., Karpiński B., Szkodo M., Selection of material for X-ray tomography analysis and DEM simulations: comparison between granular materials of biological and non-biological origins, *Granul. Matter*, (2018) 20, 38.
- [2]. Bartusek K., Fiala P., Mikulka J., Numerical modeling of magnetic field deformation as related to susceptibility measured with an MR system, *Radioengineering* (2008) 17, 113–118.
- [3]. Kłosowski G., Rymarczyk T., Gola A., Increasing the Reliability of Flood Embankments with Neural Imaging Method, *Appl. Sci.* (2018) 8, 1457.
- [4]. Rymarczyk T., Kłosowski G., Cieplak T., Kozłowski E. Application of a neural EIT system to control the processes. In *Proceedings of the 2018 Applications of Electromagnetics in Modern Techniques and Medicine PTZE 2018*, (2018).
- [5]. Banasiak R., Wajman R., Jaworski T., Fiderek P., Fidos H., Nowakowski J., Sankowski D. Study on two-phase flow regime visualization and identification using 3D electrical capacitance tomography and fuzzy-logic classification, *Int. J. Multiph. Flow* (2014) 58, 1–14.
- [6]. Garbaa H., Jackowska-Strumiłło L., Grudzień K., Romanowski A., Application of electrical capacitance tomography and artificial neural networks to rapid estimation of cylindrical shape parameters of industrial flow structure, *Arch. Electr. Eng.* (2016) 65, 657–669.
- [7]. Kryszyn J., Smolik W., Toolbox for 3D modelling and image reconstruction in electrical capacitance tomography, *Informatics Control Meas. Econ. Environ. Prot.*, (2017).
- [8]. Kryszyn J., Wanta D.M., Smolik W.T., Gain Adjustment for Signal-to-Noise Ratio Improvement in Electrical Capacitance Tomography System EVT4, *IEEE Sens. J.*, (2017) 17, 8107–8116.
- [9]. Majchrowicz M., Kapusta P., Jackowska-Strumiłło L., Sankowski D., Acceleration of image reconstruction process in the electrical capacitance tomography 3D in heterogeneous multi-GPU system, *Informatics Control Meas. Econ. Environ. Prot.*, (2017) 7, 37–41.
- [10]. Wajman R., Fiderek P., Fidos H., Jaworski T., Nowakowski J., Sankowski D., Banasiak R., Metrological evaluation of a 3D electrical capacitance tomography measurement system for two-phase flow fraction determination, *Meas. Sci. Technol.*, (2013).
- [11]. Ziolkowski M., Gratkowski S., Zywicka A.R., Analytical and numerical models of the magnetoacoustic tomography with magnetic induction, *COMPEL - Int. J. Comput. Math. Electr. Electron. Eng.*, (2018) 37, 538–548.
- [12]. Rymarczyk T., Kłosowski G. Innovative methods of neural reconstruction for tomographic images in maintenance of tank industrial reactors. *Eksplatacja i Niezawodność – Maintenance and Reliability*, 21 (2019); No. 2, 261–267
- [13]. Rymarczyk, T.; Kozłowski, E.; Kłosowski, G.; Niderla, K. Logistic Regression for Machine Learning in Process Tomography, *Sensors*, 19 (2019), 3400.
- [14]. Romanowski, A.; Łuczak, P.; Grudzień, K. X-ray Imaging Analysis of Silo Flow Parameters Based on Trace Particles Using Targeted Crowdsourcing, *Sensors*, 19 (2019), No. 15, 3317
- [15]. Valis D., Mazurkiewicz D., Application of selected Levy processes for degradation modelling of long range mine belt using real-time data, archives of civil and mechanical engineering, 18 (2018), No. 4, 1430-1440
- [16]. Kryszyn J., Smolik W., Toolbox for 3d modelling and image reconstruction in electrical capacitance tomography, *Informatyka, Automatyka, Pomiary w Gospodarce i Ochronie Środowiska (IAPGOŚ)*, 7 (2017), No. 1, 137-145
- [17]. Mosorow V., Grudzień K., Sankowski D., Flow velocity measurement methods using electrical capacitance tomography, *Informatyka, Automatyka, Pomiary w Gospodarce i Ochronie Środowiska (IAPGOŚ)*, 7 (2017), No.1, 30-36
- [18]. Galazka-Czarnecka, I.; Korzeniewska E., Czarnecki A. et al., Evaluation of Quality of Eggs from Hens Kept in Caged and Free-Range Systems Using Traditional Methods and Ultra-Weak Luminescence, *Applied sciences-basel*, 9 (2019), No. 12, 2430.
- [19]. Szczyński A., Korzeniewska E., Selection of the method for the earthing resistance measurement, *Przegląd Elektrotechniczny*, 94 (2018), No. 12, 178-181.
- [20]. Majumdar A., An autoencoder based formulation for compressed sensing reconstruction, *Magn. Reson. Imaging*, (2018) 52, 62–68.
- [21]. Ferles C., Papanikolaou Y., Naidoo K.J., Denoising Autoencoder Self-Organizing Map (DASOM), *Neural Networks*, (2018) 105, 112–131.
- [22]. Olshausen B.A., Field D.J., Sparse coding with an overcomplete basis set: A strategy employed by V1?, *Vision Res.*, (1997) 37, 3311–3325.